SUBMITTED TO APJ
Preprint typeset using LaTeX style emulateapj v. 11/10/09

arXiv:1003.4256v2 [astro-ph.CO] 3 Jun 2010

SIMULATIONS OF THE SUNYAEV-ZEL'DOVICH POWER SPECTRUM WITH AGN FEEDBACK

N. BATTAGLIA[1,2], J. R. BOND[2], C. PFROMMER[2], J. L. SIEVERS[2] AND D. SIJACKI[3]

Submitted to ApJ

ABSTRACT

We explore how radiative cooling, supernova feedback, cosmic rays and a new model of the energetic feedback from active galactic nuclei (AGN) affect the thermal and kinetic Sunyaev-Zel'dovich (SZ) power spectra. To do this, we use a suite of hydrodynamical TreePM-SPH simulations of the cosmic web in large periodic boxes and tailored higher resolution simulations of individual galaxy clusters. Our AGN feedback simulations match the recent universal pressure profile and cluster mass scaling relations of the REXCESS X-ray cluster sample better than previous analytical or numerical approaches. For multipoles $\ell \lesssim 2000$, our power spectra with and without enhanced feedback are similar, suggesting theoretical uncertainties over that range are relatively small, although current analytic and semi-analytic approaches overestimate this SZ power. We find the power at high $2000 - 10000$ multipoles which ACT and SPT probe is sensitive to the feedback prescription, hence can constrain the theory of intracluster gas, in particular for the highly uncertain redshifts > 0.8. The apparent tension between σ_8 from primary cosmic microwave background power and from analytic SZ spectra inferred using ACT and SPT data is lessened with our AGN feedback spectra.

Subject headings: Cosmic Microwave Background — Cosmology: Theory — Galaxies: Clusters: General — Large-Scale Structure of Universe — Black Hole Physics — Methods: Numerical

1. SZ POWER TEMPLATES AND THE OVERCOOLING PROBLEM

When CMB photons are Compton-scattered by hot electrons, they gain energy, giving a spectral decrement in thermodynamic temperature below $\nu \approx 220$ GHz, and an excess above (Sunyaev & Zeldovich 1970). The high electron pressures in the intracluster medium (ICM) result in cluster gas dominating the effect. The integrated signal is proportional to the cluster thermal energy and the differential signal probes the pressure profile. The SZ sky is therefore an effective tool for constraining the internal physics of clusters and cosmic parameters associated with the growth of structure, in particular the *rms* amplitude of the (linear) density power spectrum on cluster-mass scales σ_8 (e.g., Birkinshaw 1999; Carlstrom et al. 2002). Identifying clusters through blind SZ surveys and measuring the SZ power spectrum have been long term goals in CMB research, and are reaching fruition through the South Pole Telescope, SPT (Lueker et al. 2009) and Atacama Cosmology Telescope, ACT (Fowler et al. 2010) experiments. The ability to determine cosmological parameters from these SZ measurements is limited by the systematic uncertainty in theoretical modelling of the underlying cluster physics and hence of the SZ power spectrum. The power contribution due to the kinetic SZ (kSZ) effect that arises from ionized gas motions with respect to the CMB rest frame adds additional uncertainty.

There are two main approaches to theoretical computations of the thermal SZ (tSZ) power spectrum: from hydrodynamical simulations of SZ sky maps or from semi-analytical estimates (Bond et al. 2002, 2005, B0205). Large cosmological simulations providing a gastrophysical solution to the pressure distribution should include effects of non-virialized motions, accretion shocks, and deviations from spherical symmetry. Averaging over many realizations of synthetic SZ sky projections yields the power spectrum and its variance (e.g., B0205; da Silva et al. 2000; Springel et al. 2001; Seljak et al. 2001; Schäfer et al. 2006). In conjunction with primary anisotropy signals and extragalactic source models, the SZ power spectrum has been used as a template with variable amplitude $A_{\rm SZ}$ for extracting cosmological parameters by the Cosmic Background Imager (CBI) team (B0205; Sievers et al. 2009) and the ACBAR team (Goldstein et al. 2003; Reichardt et al. 2009). $A_{\rm SZ}$ was used to estimate a $\sigma_{8,\rm SZ} \propto A_{\rm SZ}^{1/7}$ as a way to encode tension between the SZ-determined value and the (lower) σ_8 obtained from the primary anisotropy signal. The CBI team also has included an analytic model (Komatsu & Seljak 2002, KS) which was also the one adopted by the WMAP team (Spergel et al. 2007). The KS template yielded a lower value for $\sigma_{8,\rm SZ}$ than that obtained with the simulation template, by $\sim 10\%$. The KS model assumes a universal ICM pressure profile in hydrostatic equilibrium with a polytropic (constant Γ) equation of state. The power spectrum is then obtained using an analytic fit to 'halo model' abundances. So far the SPT and ACT have only used the KS template and a related semi-analytic one (Ostriker et al. 2005; Bode et al. 2009). This model (Sehgal et al. 2010, S10) allows map generation by painting dark matter halos in N-body simulations with gas. It expands on KS by calculating the gravitational potential from the DM particles, includes an effective infall pressure, adds simplified models for star formation, non-thermal pressure support and energy feedback which are calibrated to observations. Using these templates, the SPT team derived a $\sigma_{8,\rm SZ}$ lower than the primary anisotropy σ_8 (e.g., WMAP7, Larson et al. 2010).

Current simulations with *only* radiative cooling and supernova feedback excessively over-cool cluster centers (e.g. Lewis et al. 2000), leading to too many stars in the core, an unphysical rearrangement of the thermal and hydrodynamic structure, and problems when compared to observations, in particular for the entropy and pressure pro-

[1] Department of Astronomy and Astrophysics, University of Toronto, 50 St George , Toronto ON, M5S 3H4.
[2] Canadian Institute for Theoretical Astrophysics, 60 St George , Toronto ON, M5S 3H8
[3] Kavli Institute for Cosmology, Cambridge and Institute of Astronomy, Madingley Road, Cambridge, CB3 0HA, United Kingdom

files. The average ICM pressure profile found through X-ray observations of a sample of nearby galaxy clusters (Arnaud et al. 2009) is inconsistent with adaptive-mesh cluster simulations (Nagai et al. 2007), as well as the KS analytic model (Komatsu et al. 2010). Pre-heating (e.g. Bialek et al. 2001) and AGN feedback (e.g. Sijacki et al. 2007, 2008; Puchwein et al. 2008) help solve the over-cooling problem and improve agreement with observed cluster properties.

Previously, an analytical model by Roychowdhury et al. (2005) has explored the effects of effervescent heating on the SZ power spectrum and Holder et al. (2007) use a semi-analytical model to calculate how an entropy floor affects the SZ power spectrum. There have been several simulations on galaxy and group scales that have studied how 'quasar' feedback impacts the total SZ decrement (Thacker et al. 2006; Scannapieco et al. 2008; Bhattacharya et al. 2008; Chatterjee et al. 2008). In this work we explore whether AGN feedback incorporated into hydrodynamical simulations of structure formation can suppress the over-cooling problem and resolve the current inconsistency between theoretical predictions and observations of the SZ power spectrum and X-ray pressure profile.

2. MODELED PHYSICS IN OUR SIMULATIONS

2.1. *Cosmological simulations*

We pursue two complementary approaches using smoothed particle hydrodynamic (SPH) simulations: large-scale periodic boxes provide us with the necessary statistics and volume to measure the SZ power spectrum; individual cluster computations allow us to address over-cooling at higher resolution and compare our AGN feedback prescription with previous models. We used a modified version of the GADGET-2 (Springel 2005) code. Our sequence of periodic boxes had sizes $100, 165, 330\,h^{-1}\,\mathrm{Mpc}$. The latter two used $N_{\rm DM} = N_{\rm gas} = 256^3$ and 512^3, maintaining the same gas particle mass $m_{\rm gas} = 3.2 \times 10^9\,h^{-1}\,\mathrm{M}_\odot$, DM particle mass $m_{\rm DM} = 1.54 \times 10^{10}\,h^{-1}\,\mathrm{M}_\odot$ and a minimum gravitational smoothing length $\varepsilon_{\rm s} = 20\,h^{-1}\,\mathrm{kpc}$; our SPH densities were computed with 32 neighbours. For our standard calculations, we adopt a tilted ΛCDM cosmology, with total matter density (in units of the critical) $\Omega_{\rm m} = \Omega_{\rm DM} + \Omega_{\rm b} = 0.25$, baryon density $\Omega_{\rm b} = 0.043$, cosmological constant $\Omega_\Lambda = 0.75$, Hubble parameter $h = 0.72$ in units of $100\,\mathrm{km\,s^{-1}\,Mpc^{-1}}$, spectral index of the primordial power-spectrum $n_{\rm s} = 0.96$ and $\sigma_8 = 0.8$. For the 'zoomed' cases (Katz & White 1993), we repeatedly simulated the cluster 'g676'(with the high resolution $m_{\rm gas} = 1.7 \times 10^8\,h^{-1}\,\mathrm{M}_\odot$, $m_{\rm DM} = 1.13 \times 10^9\,h^{-1}\,\mathrm{M}_\odot$ and $\varepsilon_{\rm s} = 5\,h^{-1}$ kpc, using 48 neighbours to compute SPH densities, as in Pfrommer et al. 2007).

We show results for three variants of gas heating: (1) the classic non-radiative 'adiabatic' case with only formation *shock heating*; (2) an extended *radiative cooling* case with star formation, supernova (SN) feedback and cosmic rays (CRs) from structure formation shocks; (3) *AGN feedback* in addition to radiative cooling, star formation, and SN feedback. Radiative cooling and heating were computed assuming an optically thin gas of a pure hydrogen and helium primordial composition in a time-dependent, spatially uniform ultraviolet background. Star formation and supernovae feedback were modelled using the hybrid multiphase model for the interstellar medium of Springel & Hernquist (2003a). The CR population is modelled as a relativistic population of protons described by an isotropic power-law distribution function in momentum space with a spectral index of $\alpha = 2.3$, following Enßlin et al. (2007). With those parameters, the CR pressure modifies the SZ effect at most at the percent level and causes a reduction of the resulting integrated Compton-y parameter (Pfrommer et al. 2007).

2.2. *AGN feedback model*

Current state-of-the-art cosmological simulations are still unable to span the large range of scales needed to resolve black hole accretion. Hence a compromise treatment for AGN feedback is needed. For example, Sijacki et al. (2007) and Booth & Schaye (2009) adopted estimates of black hole accretion rates based on the Bondi-Hoyle-Lyttleton formula (Bondi & Hoyle 1944). Here we introduce a sub-grid AGN feedback prescription for clusters that allows for lower resolution still and hence can be applied to large-scale structure simulations. We couple the black hole accretion rate to the global star formation rate (SFR) of the cluster, as suggested by Thompson et al. (2005) using the following arguments. The typical black hole accretion rates and masses for the inner gravitationally stable AGN disks (of size $\lesssim 1$pc) are $\sim 1\,\mathrm{M}_\odot/\mathrm{yr}$ and $\sim 10^6\,\mathrm{M}_\odot$. Since AGN lifetimes are much longer than 1 Myr, mass must be transferred from larger radii to the inner disk. However, at much larger radii this outer disk is gravitationally unstable and must be forming stars. Thus, in order to feed the AGN, stability arguments suggest that the rate of accretion must be greater than the SFR. For simplicity we assume that $\dot{M}_{\rm BH} \propto \dot{M}_\star$. We inject energy into the ICM over a spherical region of size $R_{\rm AGN}$ about the AGN, according to

$$E_{\rm inj}(< R_{\rm AGN}) = \varepsilon_{\rm r}\dot{M}_\star(< R_{\rm AGN})c^2\Delta t \quad \text{if } \dot{M}_\star(< R_{\rm AGN}) > 5\,\mathrm{M}_\odot/\mathrm{yr}\,. \tag{1}$$

The duty cycle over which the AGN outputs energy is Δt and $\varepsilon_{\rm r}$ is an 'efficiency parameter'. (As we describe below, the calculated efficiency for turning mass into energy is much smaller than $\varepsilon_{\rm r}$.) We have explored a wide range of our two parameters, but the specific choices made for the figures are $\Delta t = 10^8$ yr and $\varepsilon_{\rm r} = 2 \times 10^{-4}$. We require a minimum SFR of $5\,\mathrm{M}_\odot/\mathrm{yr}$ to activate AGN heating in the halo it is housed in.

Given the output AGN energy, we must prescribe how it is to be distributed. Our procedure is motivated by the way Sijacki & Springel (2006) did AGN heating via bubbles. Using an on-the-fly friends-of-friends (FOF) halo finding algorithm in GADGET-2, we determine the mass and center of mass of each halo with $M_{\rm halo} > 1.2 \times 10^{12}\,h^{-1}\,\mathrm{M}_\odot$. We calculate its global SFR within the AGN sphere of influence of radius

$$R_{\rm AGN} = \max\left\{\left[\frac{M_{\rm halo}}{10^{15}\,h^{-1}\,\mathrm{M}_\odot}\right]^{1/3}[E(z)]^{-2/3}, \frac{u_{\rm AGN}}{1+z}\right\} \times 100\,h^{-1}\,\mathrm{kpc}, \tag{2}$$

where $u_{\rm AGN} = \varepsilon_{\rm s}$ and $E(z)^2 = \Omega_{\rm m}(1+z)^3 + \Omega_\Lambda$. Within the halos we partition $E_{\rm inj}$ onto those gas particles inside of $R_{\rm AGN}$ according to their mass. We have varied the prescription for $R_{\rm AGN}$ and its floor $u_{\rm AGN}$ (chosen here to be the gravitational softening $\varepsilon_{\rm s}$); the specific numbers given in eq. 2 (and for $\varepsilon_{\rm r}$) match previous successful models that suppress the over-cooling by means of AGN feedback (Sijacki et al. 2008, see Sect. 3.1). Defining R_Δ as the radius at which the mean interior density equals Δ times the critical density $\rho_{\rm cr}(z)$ (e.g., for $\Delta = 200$ or 500), then the ratio of $R_{\rm AGN}$ to R_{200} is a constant ~ 0.05.

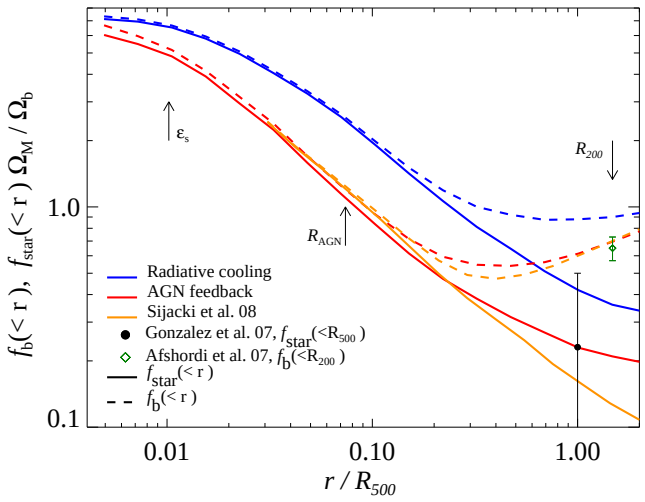

FIG. 1.— Shown are f_b (dashed lines) and f_{star} (solid lines) normalized to the universal value ($f_b = 0.13$) assumed in our simulations of our cluster g676 with $M_{500} = 6.8\times10^{13}\,h^{-1}\,M_\odot$. The blue lines are for the simulation with radiative cooling and star formation while the red and orange lines are for our AGN feedback model ($\varepsilon_r = 2\times10^{-4}$, $\dot{M}_\star \gtrsim 5\,M_\odot$/yr) and that by Sijacki et al. (2008), respectively. The data points are observations by Gonzalez et al. (2007) and Afshordi et al. (2007). $f_{star}(<R_{500})$ from X-ray measurements also agrees well, but the errors are large. Our sub-grid model matches the results from Sijacki et al. (2008) in this high resolution simulation well.

Although we have referred to our feedback mechanism as being caused by AGN outflows, radiation pressure from stellar luminosity acting on dust grains will serve much the same purpose, and could also deliver high efficiencies (e.g. Thompson et al. 2005). In the code, we have so far added E_{inj} as a pure heating component, but it should allow for a mechanical, momentum-driven wind component as well, which would not be as prone to catastrophic cooling and likely decrease the ε_r needed for useful star formation suppression.

The relevant energy budget is not in fact defined by ε_r, but rather by a redshift-dependent effective feedback efficiency $\varepsilon_{eff} \equiv \Sigma_i E_{inj,i}/[M_\star(<r)\,c^2]$, where we sum over every energy injection event (labeled by i) and we calculate the stellar mass $M_\star(<r)$ within a given radius. In all cases, $\varepsilon_{eff} \ll \varepsilon_r$, because: (i) heating suppresses the stellar mass $\Delta M_\star$ created over Δt, making it quite a bit less than the stellar mass $\dot{M}_\star\Delta t$ that would have formed without any feedback; and (ii) E_{inj} is a stochastic variable, which we find to be zero about half of the time because the required SF threshold is not achieved. With our fixed $\varepsilon_r - R_{AGN}$ prescription, our canonical g676 example has $\varepsilon_{eff} \sim 5\times10^{-6}$ for the entire simulation; if all energy had been released within the final R_{AGN}, ε_{eff} would be 8×10^{-5}, but feedback, especially at early times, is much more widely distributed. Of a total $E_{inj} = 9\times10^{61}$ ergs for g676 we find 58% is delivered in the cluster formation phases at $z > 2$, another 23% is delivered in the redshift range $1 < z < 2$ that can be probed with ACT and SPT resolution, and only 19% comes from the longer period below redshift 1. Feedback prescriptions with smaller E_{inj} which still give the desired star formation suppression need further exploration.

3. PRESSURE PROFILES

3.1. *Testing AGN feedback as resolution varies*

AGN feedback self-regulates the star formation and energetics of a cluster. In Fig. 1 we compare the fraction of baryons (f_b) and stars (f_{star}) as functions of cluster radius for the high-resolution 'g676' simulations. Our radiative simulation produces 1.5 – 2 times more stars than those with AGN feedback. Our sub-grid AGN model nicely reproduces the results in Sijacki et al. (2008). It should also produce reliable results in the cosmological box simulations in which overcooling is less severe because of the lower resolution. There is significant sensitivity to the value chosen for the feedback parameter ε_r: doubling it lowers f_b by a factor of 1.5, halving it increases f_{star} by 1.4. The $100\,h^{-1}$ Mpc simulations were used to study the resolution dependence of our feedback model by varying $N_{gas}^{1/3}$ in steps from 64 to 256, with ε_s and hence u_{AGN} (eq. 2) decreased accordingly. As u_{AGN} decreased, f_{star} within R_{500} increased almost linearly for radiative cooling, whereas for AGN feedback the increases were less. This can be traced to the hierarchical growth of structure since in low-resolution simulations: the small star forming systems are under-resolved; this decreases the SFR that mediates our AGN feedback; and this lowers the overall number of stars produced in the simulations. This behaviour is seen in other AGN feedback models (Sijacki et al. 2007) and has been extensively studied in non-AGN feedback simulations by Springel & Hernquist (2003b).

3.2. *Stacked pressure profiles*

For every halo identified by our FOF algorithm, we calculate the center of mass, R_Δ, the mass M_Δ within R_Δ and compute the spherically-averaged pressure profile normalized to $P_\Delta \equiv GM_\Delta\Delta\rho_{cr}(z)f_b/R_\Delta$, with $f_b = \Omega_b/\Omega_m$ (Voit 2005) and radii scaled by R_Δ. We then form a weighted average of these profiles for the entire sample of clusters at a given redshift. For Fig. 2, we have weighted by the integrated y-parameter,

$$Y_\Delta = \frac{\sigma_T}{(m_e c^2)}\int_0^{R_\Delta} P_e(r)4\pi r^2\,dr \propto E_{th}(<R_\Delta)\,, \qquad (3)$$

where σ_T is the Thompson cross-section, m_e is the electron mass and P_e is electron pressure. For a fully ionized medium the thermal pressure $P = P_e(5X_H+3)/2(X_H+1) = 1.932P_e$, where $X_H = 0.76$ is the primordial hydrogen mass fraction. Splitting the clusters into a number of mass bins gives similar results to this monolithic Y_Δ weight, as does weighting by Y_Δ^2. We have found that a simple parametrized model

$$P/P_{500} = A\,[1+(x/x_c)^\alpha]^{-\gamma/\alpha}\ ,\ x \equiv r/R_{500}\,, \qquad (4)$$

with core-scale x_c, amplitude A, and two power law indices, α and γ, fits better than with a fixed α. Sample values for our AGN feedback are $A = 82$, $x_c = 0.37$, $\alpha = 0.84$ and $\gamma = 4.6$ at $z = 0$; generally the parameters depend upon cluster mass and redshift. At $z \gtrsim 1$, a more complex parameterization is needed.

In Fig. 2, we show average pressure profiles multiplied by x^3 to make them $\propto dE_{th}/d\ln r$, the thermal energy per logarithmic interval in radius, and hence to $dY_\Delta/d\ln r$. All profiles of $dE_{th}/d\ln r$ from simulations and observations peak at or before R_{200}, but an integration to at least $4R_{200}$ is required for the total thermal energy to converge. By contrast, the KS profile does not drop over this range due to the constancy of Γ and does not include the outer cluster phenomena of asphericity, accretion shocks, *etc.* Throughout this paper, we have computed the KS model with an updated concentration parameter given by Duffy et al. (2008). We also show a scaled average S10 pressure profile for clusters with $10^{14}M_\odot < M_{500} < 5\times10^{14}$ and redshift < 0.2. The S10 profile

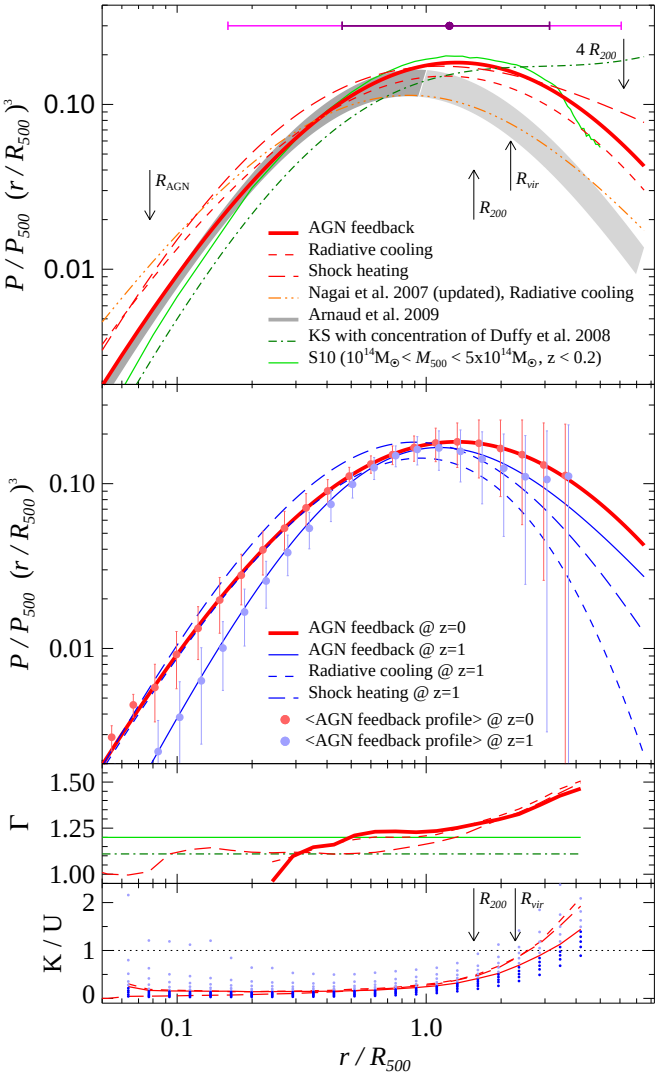

FIG. 2.— *Top:* Comparison of fits to normalized average pressure profiles from analytic calculations, simulations and observations, scaled by $(r/R_{500})^3$. For a cluster of $M_{500} = 2 \times 10^{14}\, h^{-1} M_\odot$, we show fits to our SPH simulations (red), and compare them with the analytic KS profile (green), the semi-analytic S10 average profile (light green), and a fit to AMR simulations (updated profile by Nagai et al. 2007, private communication; orange). Our feedback model matches a fit to X-ray observations (Arnaud et al. 2009, grey bands) within R_{500} well; only the dark grey part is actually a fit to the data, with the light grey their extrapolation using older theory results unrelated to the data. We illustrate the 1 and 2 σ contributions to Y_Δ centered on the median for the feedback simulation by horizontal purple and pink error bars. *2nd panel:* We compare fits to our AGN model at redshift $z = 0$ (red solid) to all our three models at redshift $z = 1$ (blue). Shown are the 1σ error bars of the cluster-by-cluster variance of the weighted averages in our AGN models using corresponding lighter colors. *3rd panel:* We show the effective adiabatic index Γ for our simulations, comparing it with KS (dash-dotted) and with a constant 1.2 (light green). *Bottom:* The distribution of kinetic-to-thermal energy in percentile decades is indicated by the dots for the feedback case, with the median shown for all three models; thus, there are significant additions to pressure support even in the cores of simulated clusters, and even more so in the SZ-significant outer parts.

has been weighted by Y_Δ and agrees well within R_{500} and with a slight excess pressure beyond R_{500}.

Fig. 2 shows our feedback model traces the observed "universal" X-ray profile of Arnaud et al. (2009) shown as a dark-grey band rather well within R_{500}. This fit came out naturally, with no further tuning of our feedback parameters beyond trying to agree with the Sijacki et al. (2008) simulation. Our models without AGN feedback have larger pressures inside R_{500}. For the light grey band beyond R_{500}, the universal X-ray profile did not use observations, but was fit to an average profile of earlier simulations so the deviation > R_{500} does not represent a conflict of our profiles with the data, rather with the earlier simulations. The band shown for the X-ray profile gives a crude correction for the bias in M_{500} and R_{500} resulting from the Arnaud et al. (2009) assumption of hydrostatic equilibrium. This yields mass values which are on average 25% too low (Nagai et al. 2007), so the band represents a 0-25% uncertainty in M_{500}. This change only affects $R_{500} \propto M_{500}^{1/3}$ and $P_{500}R_{500}^3 \propto M_{500}^{5/3}$ but does not affect the shape of the profile. (However, as the bottom panel shows, such a correction from turbulence and un-virialized bulk motions (Kravtsov et al. 2006) will depend upon radius and selection function of the X-ray clusters used to make the fit.)

Another important issue is the relation between the Y_Δ and cluster mass. We fit our results for this to the scaling relation

$$Y_{500} = 10^B\, (M_{500}/3 \times 10^{14}\, h_{70}^{-1}\, M_\odot)^A\, h_{70}^{-5/2}\, \mathrm{Mpc}^2, \qquad (5)$$

where $h_{70} \equiv 0.7 \times 100$ km s^{-1} Mpc^{-1}. Parameters from our simulation are $B = (-4.47 \pm 0.08, -4.46 \pm 0.20, -4.5 \pm 0.1)$ and $A = (1.66 \pm 0.12, 1.71 \pm 0.25, 1.75 \pm 0.06)$ for the sequence (1) shock heating, (2) radiative cooling and (3) AGN feedback. These values are similar to the $B = -4.739 \pm 0.003$ and $A = 1.790 \pm 0.015$ found by Arnaud et al. (2009), as well as the $B = -4.713 \pm 0.004$ and $A = 1.668 \pm 0.009$ found by S10. We note that Arnaud et al. (2009) actually used a mass proxy in place of M_{500}, so their errors are not representative of the true observational scatter in the $Y-M$ scaling relation. The AGN feedback model of Sijacki et al. (2007) was also able to reconcile the cluster X-ray luminosity and temperature scaling relation (Puchwein et al. 2008).

We find a large variation in the outer pressure profiles beyond $R_{\rm vir}$, especially at redshift $z \sim 1$ as is shown in the second panel of Fig. 2. These regions may have sub-halos, and external but nearby groups on filaments, most of which will eventually be drawn into the clusters. In spite of the large variance of the scaled profiles, the fit to the profiles at $z = 0$ follows the average. At larger redshift, however, our fitting formula will require more degrees of freedom than in eq. 5 to reflect the range of behaviour of the highly dynamical outer regions.

4. SZ POWER SPECTRA FROM HYDRODYNAMICAL SIMULATIONS

4.1. *Stacked SZ power spectra of translated-rotated cosmological boxes*

We randomly rotate and translate our simulation snapshots at different redshifts (da Silva et al. 2000; Springel et al. 2001, B0205). To obtain thermal Compton-y maps, we perform a line-of-sight integration of the electron pressure within a given solid angle, i.e. $y = \sigma_{\rm T} \int n_{\rm e} k\, T_{\rm e}/(m_{\rm e}c^2)\, {\rm d}l$, where k is the Boltzmann constant, $n_{\rm e}$ and $T_{\rm e}$ are the number density and temperature, respectively. We construct 1.6°×1.6°and 3.2°×3.2°maps for the 256^3 and 512^3 simulations, respectively. Using this method there are large sample variances (White et al. 2002) associated with nearby cluster contamination. We have quantified their influence on the power spectrum for each of our three physics models by averaging over twelve translate-rotate viewing angles each projected from our ten 256^3 full hydrodynamical simulations for each of the 33 redshift outputs back to a redshift $z = 5$; the power spectra of which are then added up to yield the total spectrum. This

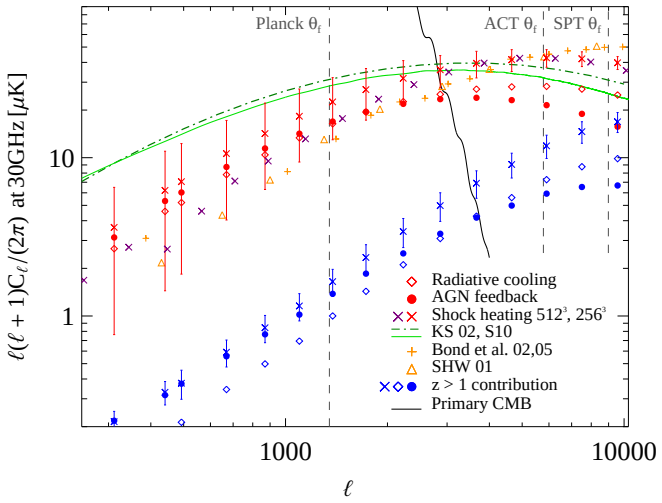

FIG. 3.— Predictions for the tSZ power spectrum at 30 GHz from our simulations (red and purple symbols), simulations by Springel et al. (2001) (orange triangles), simulations by Bond et al. (2005) (orange pluses), semi-analytical simulations by S10 (dark green) and analytical calculations by KS (light green). The 256^3 power spectra (red symbols) are averages over 12 translate-rotate tSZ maps and 10 separate hydrodynamical simulations for each of the 33 redshift bins, the power spectra of which are then added up to yield the total spectrum; the error bars show the variance among the power in all maps. The full-width half-max values appropriate for Planck, ACT and SPT show which part of the templates these experiments are sensitive to. At low-ℓ, the discrepant higher power in the semi-analytical calculations can be traced to the enhanced pressure structures assumed beyond R_{200} over what we find.

method of computing the power spectrum has the advantage of taking care of the artificial correlations that occur because any individual simulation follows the time evolution of the same structure. For the shock heating case, we did ten more hydrodynamical simulations to show that our averaged template had converged (within ~10%), but note that using only a few boxes can be misleading in terms of rare events.

The computationally more expensive 512^3 SZ spectra have the equivalent of 8 256^3 plus wider coverage, so the 512^3 shock heating result shown gives a reasonable indication of what to expect. The other 2 physics single-box cases at 512^3 are similar to the 256^3 ensemble means. The analytical approach has the great advantage of including an accurate mean cluster density to high halo masses, but to be usable for SZ power estimation, scaled pressure profiles must also be accurate, a subject we turn to in future work. For now, we note that using such profiles from our simulations gives good agreement with the average SZ power shown at the low ℓ where sample variance will be largest. In Fig. 3, our simulation templates and the KS template shown have excluded structures below $z = 0.07$ to decrease the large sample variance associated with whether a large-ish cluster enters the field-of-view. Such entities would typically be removed from CMB fields and considered separately.

The mean Compton y-parameter found in our AGN feedback simulations is one order of magnitude below the COBE FIRAS upper limit of 15×10^{-6} (Fixsen et al. 1996).

We compare the theoretical predictions for the tSZ power spectrum in Fig. 3. Our 512^3 and 256^3 shock heating simulations are in agreement with previous SPH simulation power spectra (Springel et al. 2001, B0205) scaled by $C_\ell \propto (\Omega_b h)^2 \Omega_m \sigma_8^7$, with the factors determined from our simulations of differing cosmologies. The B0205 SZ power shown had a cut at $z = 0.2$, appropriate for CBI fields; using the same cut on a shock heating simulation with the same cosmology that we have done, we get superb agreement.

The KS and S10 semi-analytic SZ power spectra templates differ substantially from our templates, in particular with higher power at low ℓ: as shown in Fig. 2, the KS pressure profile beyond R_{500} overestimates the pressure relative to both simulations and observations, leading to the modified shape and larger Y_Δ; this behaviour is also shown in Komatsu et al. (2010). The spectrum from S10 is very similar to KS possibly because both assume hydrostatic equilibrium, and a polytropic equation of state with a fixed adiabatic index, $\Gamma \sim 1.1 - 1.2$. Inside R_{200}, these assumptions are approximately correct, but they start to fail beyond R_{200}. A demonstration of this is the rising of Γ and of the ratio of kinetic-to-thermal energy K/U shown for our simulations in the bottom panels of Fig. 3. The present day ($a = 1$) internal kinetic energy of a cluster is given by $K \equiv \Sigma_i m_{\mathrm{gas},i} |\boldsymbol{v}_i - \bar{\boldsymbol{v}} + H_0(\boldsymbol{x}_i - \bar{\boldsymbol{x}})|^2 /2$, where H_0 is the present day Hubble constant, $\boldsymbol{v}_i$ and $\boldsymbol{x}_i$ are the peculiar velocity and comoving position for particle i, and $\bar{\boldsymbol{v}}$ and $\bar{\boldsymbol{x}}$ are the gas-particle-averaged bulk flow and center of mass of the cluster. The additional thermal pressure support we find at large radii from AGN feedback results in the slightly slower rate of K/U growth shown. In all cases the large kinetic contribution shown should be properly treated in future semi-analytic models.

Varying the physics over the three cases for energy injection in our simulations leads to relatively minor differences in Fig. 3 among the power spectra for $\ell \lesssim 2000$. This agreement is due in part to hydrostatic readjustment of the structure so the virial relation holds, which relates the thermal content, hence Y_Δ, to the gravitational energy, which is dominated by the dark matter. Our AGN feedback parameters do not lead to dramatic gas expulsions to upset this simple reasoning. Our radiative cooling template has less power at all scales compared to the shock heating template since baryons are converted into stars predominantly at the cluster centers and the ICM adjusts adiabatically to this change. Thus, at low ℓ where clusters are unresolved, shock heating and radiative simulations give upper and lower limits, bracketing the AGN feedback case. AGN feedback suppresses the core value of the pressure compared to the radiative simulation resulting in less power at $\ell > 2000$, a trend that is more pronounced at $z > 1$ (as shown in Fig. 3). Thus, at these angular scales, the power spectrum probes the shape of the average pressure profile. It depends sensitively on the physics of star and galaxy formation e.g., Scannapieco et al. (2008). Over the ℓ-range covered by Planck, these effects are sub-dominant, and serve to highlight the importance of the high-resolution reached by ACT and SPT.

4.2. *Current constraints on SZ template amplitudes and* $\sigma_{8,\mathrm{SZ}}$

Instead of varying all cosmological parameters on which the thermal and kinetic SZ power spectra, $C_{\ell,\mathrm{tSZ}}$ and $C_{\ell,\mathrm{kSZ}}$, depend, we freeze the shapes by adopting the parameters for our fiducial $\sigma_8 = 0.8$ (and $\Omega_b h = 0.03096$) model evaluated at 150 GHz, and content ourselves with determining template amplitudes, A_{tSZ} and A_{kSZ}, and a total SZ amplitude A_{SZ}:

$$A_{\mathrm{SZ}} C_{\ell,\mathrm{SZ}} \equiv f(\nu) A_{\mathrm{tSZ}} C_{\ell,\mathrm{tSZ}} + A_{\mathrm{kSZ}} C_{\ell,\mathrm{kSZ}} \,. \qquad (6)$$

The spectral function for the tSZ (Sunyaev & Zeldovich 1970), $f(\nu)$, vanishes at the SZ null at ~ 220 GHz and we normalize it to unity at $\nu = 150$ GHz, so it rises to 4 at 30 GHz. Therefore if we find values of A_{SZ} below unity then either σ_8 is smaller than the fiducial cosmological value as

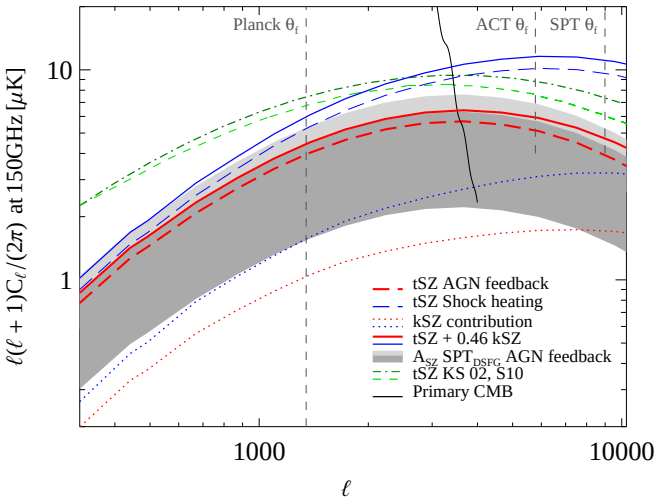

FIG. 4.— Our 150 GHz tSZ adiabatic and feedback (A_{SZ} = 1) power spectra computed with σ_8 = 0.8 (long dashed lines) are contrasted with the dark grey band indicating the 1σ range in multiplicative amplitude, $A_{SZ} = 0.75 \pm 0.36$, allowed by the SPT_{DSFG} power spectrum for the feedback template shape. The light grey band is the 2σ upper limit region. The A_{SZ} = 1 S10 tSZ power spectrum (dashed line) and the KS tSZ spectrum (dash dotted line) are shown for contrast; their allowed 1σ band is determined by multiplying these by their A_{SZ} values given in Table 1, but cover a similar swath to the grey bands. We also show the averaged kSZ power spectra computed for our simulations by dotted lines. The kSZ spectra were calculated in the same was as the tSZ spectra were, and have similar shapes. However, kSZ is underestimated at low ℓ because of missing bulk velocities in the simulations. There should be an additional (rather uncertain) kSZ template from inhomogeneous reionization as well. To show the tension with the CMB data, we plot the tSZ + 0.46 kSZ power (solid lines) since this can be directly compared with the SPT_{DSFG} grey bands.

derived from the primary CMB anisotropies, or else the theoretical templates overestimate the SZ signal.

To determine the probability distributions of these amplitudes and other cosmological parameters from current CMB data we adopt Markov Chain Monte Carlo (MCMC) techniques using a modified version of CosmoMC (Lewis & Bridle 2002). We include WMAP7 (Larson et al. 2010) and, separately, ACT (Fowler et al. 2010) and SPT (Lueker et al. 2009). In all cases, we assume spatial flatness and fit for 6 basic cosmological parameters ($\Omega_b h^2$, $\Omega_{DM} h^2$, n_s, the primordial scalar power spectrum amplitude A_s, the Compton depth to re-ionization τ, and the angular parameter characterizing the sound crossing distance at recombination θ). We also allow for a flat white noise template $C_{\ell,src}$ with amplitude A_{src}, such as would arise from populations of unresolved point sources. We marginalize over A_{src}, allowing for arbitrary (positive) values. Generally there will also be a spatial clustering component for such sources, and these will have templates that are partially degenerate in shape with that for tSZ, but because of the large uncertainties we ignore such contributions here. Reducing the SZ and unresolved source problems to determinations of overall amplitudes multiplying shapes has a long history, e.g., the CBI sequence of papers, and was adopted as well by the ACT and SPT teams. Our results differ slightly from those reported by the ACT team because they use WMAP5+ACT and a combined tSZ+kSZ S10-template, and by the SPT team who use WMAP5+QUaD+ACBAR+SPT and add constraints on the white noise source amplitude beyond the non-negativity we impose.

We first consider a simplified case with A_{kSZ} constrained to be zero and all other cosmic parameters and the source amplitude marginalized, yielding a probability distribution for A_{SZ}. The means and standard deviations from our MCMC runs are given in the upper rows of Table 1 in columns 2, 4 and 6 for a number of data combinations and for our 3 physics simulation cases, contrasting with KS and S10. The ACT data is for 148 GHz. There are two SPT cases given. The first uses just the 153 GHz spectrum so it can be directly compared to ACT. For SPT, Lueker et al. (2009) also report a power spectrum derived from subtracting a fraction x of their 220 GHz data from the 153 GHz data to minimize the contribution from dusty star-forming galaxies (DSFG); since 220 GHz is the SZ null, this does not modify the tSZ contribution, but would diminish the frequency-flat kSZ. However, a normalization factor is chosen to preserve power for primary CMB signals that are flat in frequency like kSZ. This has the effect of boosting the tSZ power by a factor of $(1-x)^{-2}$. Lueker et al. (2009) find that $x = 0.325$ minimizes the contribution from the DSFGs so the DSFG-subtracted spectrum suppresses the kSZ by a factor of 0.46 relative to the tSZ. A ~25% uncertainty remains in x which should be taken into account statistically, but is not here. The correct approach would be to simultaneously treat the 153 GHz and 220 GHz cases, with full modelling of the different classes of point sources, including their clustering, and to take into account the non-Gaussian nature of the SZ and source signals which impact sample variance.

The ACT data is only giving upper limits with their current published data, whereas SPT has detections at 153 GHz with A_{SZ} compatible with unity. For the SPT 153 GHz-only spectrum, we find S10 gives $A_{SZ} = 1.39 \pm 0.34$ while the feedback template gives $A_{SZ} = 1.76 \pm 0.43$, and the comparable 95% upper limits from ACT are 1.95 and 2.93. However, although the white noise shape has been vetoed by marginalization, there could be a residual clustered source contribution from dusty galaxies pushing the derived A_{SZ} high. To the extent that SPT_{DSFG} vetoes this DSFG clustering as well as their Poisson contribution, that A_{SZ} would be a better indicator. It shifts from 0.43 ± 0.21 for KS and 0.50 ± 0.25 for S10 up to 0.75 ± 0.36 for the feedback template, an increase of 50%. The large difference between the 150 and source-subtracted templates, even after marginalizing over a Poisson term, may suggest the power in the correlated source component may be similar to the SZ power, emphasizing the work necessary to do a correct treatment.

Any non-zero kSZ contribution will take some of the amplitude from A_{SZ}, leaving even smaller A_{tSZ} values; columns 3, 5 and 7 of the table give estimates of this diminution. The kSZ power spectra that we have computed are broadly similar to the tSZ power shape, with however sufficiently significant differences to allow shape discrimination in addition to the frequency separability, as Fig. 4 shows. At 150 GHz and an ℓ = 3000 pivot, we find the kSZ power is ~ 29%, ~ 29% and ~ 27% of the tSZ power for the shock heating, radiative cooling and feedback simulations, respectively. We normalize the kSZ to the tSZ at this pivot of 3000 since it has most of the constraining power in the CosmoMC chains for the ACT and SPT measurements and results in the smallest error bars: on larger scales, the errors are increased by the contribution from primary anisotropies while smaller scales are dominated by the instrumental and galaxy-source shot noise.

We used exactly the same procedure to obtain the kSZ spectrum as we used for the tSZ spectrum. The temperature decrement due to the kSZ effect is $\Delta T/T = \sigma_T \int n_e \, v_r/c \, dl$, where v_r is the radial peculiar velocity of the gas relative to

TABLE 1
CONSTRAINTS ON A_{SZ} AND $\sigma_{8,SZ}$

tSZ template	ACT 148 GHz		SPT 153 GHz		SPT_{DSFG}	
	A_{SZ}	A_{tSZ}	A_{SZ}	A_{tSZ}	A_{SZ}	A_{tSZ}
KS	< 1.55	< 1.26	1.01 ± 0.25	0.72 ± 0.25	0.43 ± 0.21	0.30 ± 0.21
S10	< 1.95	< 1.67	1.39 ± 0.34	1.11 ± 0.34	0.50 ± 0.25	0.38 ± 0.25
Shock heating	< 2.13	< 1.84	1.13 ± 0.28	0.84 ± 0.28	0.44 ± 0.22	0.31 ± 0.22
Radiative cooling	< 2.75	< 2.46	1.50 ± 0.37	1.21 ± 0.37	0.59 ± 0.29	0.45 ± 0.29
Feedback	< 2.93	< 2.66	1.76 ± 0.43	1.49 ± 0.43	0.75 ± 0.36	0.63 ± 0.36
	$\sigma_{8,SZ}$	$\sigma_{8,tSZ}$	$\sigma_{8,SZ}$	$\sigma_{8,tSZ}$	$\sigma_{8,SZ}$	$\sigma_{8,tSZ}$
KS	< 0.864	< 0.845	$0.792^{+0.029}_{-0.029}$	$0.757^{+0.039}_{-0.037}$	$0.690^{+0.057}_{-0.055}$	$0.622^{+0.105}_{-0.051}$
S10	< 0.891	< 0.874	$0.828^{+0.031}_{-0.030}$	$0.800^{+0.038}_{-0.036}$	$0.705^{+0.060}_{-0.058}$	$0.636^{+0.109}_{-0.054}$
Shock heating	< 0.900	< 0.883	$0.804^{+0.031}_{-0.030}$	$0.768^{+0.040}_{-0.038}$	$0.691^{+0.059}_{-0.057}$	$0.607^{+0.119}_{-0.057}$
Radiative cooling	< 0.935	< 0.922	$0.837^{+0.032}_{-0.031}$	$0.809^{+0.039}_{-0.037}$	$0.721^{+0.060}_{-0.058}$	$0.660^{+0.102}_{-0.053}$
Feedback	< 0.944	< 0.932	$0.856^{+0.033}_{-0.032}$	$0.835^{+0.038}_{-0.037}$	$0.746^{+0.061}_{-0.059}$	$0.703^{+0.091}_{-0.055}$

The mean and standard deviation of the thermal SZ power spectrum template amplitude A_{tSZ} and the total SZ, including our computed kSZ contribution. The numbers assume the kSZ template is perfectly degenerate in shape with the tSZ one. $A_{SZ} = A_{tSZ} + A_{kSZ}$ at 150 GHz, with the relative enhancement in our simulations given by $A_{kSZ}/A_{tSZ} = 0.29, 0.29, 0.27$ for the shock heating, radiative cooling and feedback simulations, respectively. We have used the ACT team's 148 GHz power spectrum, the SPT team's 153 GHz spectrum and the SPT DSFG-subtracted (SPT_{DSFG}) spectrum, along with WMAP7. The amplitude of the SZ power is normalized to our fiducial $\sigma_8 = 0.8$ cosmology. A rough guide to the σ_8 tension is obtained in the lower rows, using $\sigma_{8,SZ} \propto A_{SZ}^{1/7} (\Omega_b h)^{-2/7}$, with exponents determined by B0205 and KS. Since kSZ varies more slowly with σ_8 than tSZ, the numbers are just indicative.

the observer. We constructed 12 translate-rotate kSZ maps for each of our 10 separate hydrodynamical simulations and for each of the 41 redshift bins back to $z = 10$ (rather than $z = 5$ for tSZ), computing the average and variance of all of these. Since we use simulations with side length $L = 165\,h^{-1}$Mpc for our 256^3 cases, with fundamental wavenumber $(26\,h^{-1}\mathrm{Mpc})^{-1}$, our spectra are missing a bit of power on the largest scales (affecting low-ℓ) since we do not sample well the long-wavelength tail of the velocity power spectrum in spite of the number of runs done.

We have included the kSZ template by ignoring the relatively small shape difference about the pivot point of the kSZ and tSZ power spectra; i.e., we assume the perfect degeneracy $C_{\ell,kSZ} = C_{\ell,tSZ}$, as the SPT team did. Thus we only need the ratios A_{kSZ}/A_{tSZ} given above for the 150 GHz cases and the further x factors for the mixed frequency DSFG case. For the ratios we use our translate-rotate values of 0.29, 0.29 and 0.27 from our simulations, 0.276 for S10, and used a rough estimate of 0.25 for KS. Apart from ignoring the shape difference, we have also ignored kSZ from patchy re-ionization at high redshift, although it can have a competitive amplitude to the late time fully ionized gas motions with respect to the CMB rest frame that we are modelling (Iliev et al. 2008, 2007). In presenting the results from our analyses of the MC Markov chains, we just subtract A_{kSZ} from A_{SZ}. The Table 1 A_{tSZ} that we derive from these assumptions are all on the low side of unity for DSFG, with KS and S10 being more than 2.5σ low, whereas the feedback template is only about 1σ low (and 1σ high for 153 GHz alone). We leave it to future work to include a more complete implementation of the kSZ spectra.

The means and errors on A_{SZ} provide the cleanest way of presenting the tension, or lack thereof, of these SZ models with the primary CMB data which indicates $\sigma_8 \approx 0.8$. However, it has been conventional to translate these numbers into a $\sigma_{8,SZ}$ using the way A_{SZ} scales with cosmic parameters, roughly as $A_{SZ} \propto \sigma_8^7 (\Omega_b h)^2$, as given by B0205 and KS. The lower rows in Table 1 show $\sigma_{8,SZ}$ using this scaling. Although the scaling applies to the tSZ component only, with the kSZ power being less sensitive to σ_8, we also quote results for the kSZ-corrected cases. Ideally one should use the data to determine the cosmic parameters which uniquely and fully determine the primary spectrum, the A_{tSZ} and A_{kSZ}, and the tSZ and kSZ shape modifications as the parameters vary. This slaved treatment enforcing $\sigma_{8,SZ} = \sigma_8$ has σ_8's value being driven by WMAP7 and other primary CMB data rather than by the SZ information.

5. CONCLUSIONS AND OUTLOOK

Without hydrodynamical simulations in a cosmological framework similar to the ones presented in this paper it is hard to come up with a consistent model of the gas distribution in clusters and the infall regions which both contribute significantly to the SZ power spectrum. In this paper, we identify three main points that a future semi-analytic model of such a pressure distribution has to provide.

(1) In order to arrive at a consistent gas distribution that matches not only the integrated stellar mass fraction but also the X-ray derived pressure profiles within R_{500}, we need self-regulating AGN-type feedback. We emphasize that we tuned our parameters to match a previous single-cluster model that successfully suppressed the over-cooling by means of AGN feedback (Sijacki et al. 2008). The excellent agreement with current data was a pleasant byproduct: our simulated pressure profiles agree with recently obtained observational ones that have been constructed from X-ray data; the scaling relations between the cluster mass and X-ray based Compton-Y (Arnaud et al. 2009) also agree; as do the integrated stellar and gas mass fractions (Gonzalez et al. 2007; Afshordi et al. 2007).

(2) The amount of non-gravitational energy injection into proto-clusters and groups by AGN and starburst galaxies at intermediate-to-high redshifts $z \gtrsim 0.8$ is poorly understood. Other observables are needed to constrain the physics and to answer this question which seems to be essential in understanding the resulting gas profiles. Our simulations suggest that AGN-type feedback lowers the central pressure values as a hydrodynamic response of the gas distribution to the non-gravitational feedback of energy. This effect inhibits gas from

falling into the core regions which causes a flatter and more extended pressure profile and a noticeably reduced power of the SZ power spectrum at small angular scales for $\ell \gtrsim 2000$.

(3) For the SZ flux to be converged, an integration of the pressure profile out to $4R_{200}$ is necessary; half of the SZ flux is contributed from regions outside R_{200}. To compute a reliable SZ power spectrum, it is essential to precisely characterize the state of the gas in these infall regions. In particular, we find that: (i) the pressure support from kinetic energy strongly increases as a function of radius to reach on average equipartition with the thermal energy at $\sim 2R_{200}$ in our AGN model with the exact dependence on cluster mass to be determined by future work; (ii) the effective adiabatic index $\Gamma = \mathrm{d}\ln p/\mathrm{d}\ln\rho \sim 1.2$ in the interior, but upturns towards $\Gamma \sim 5/3$ beyond the virial radius; (iii) the inclusion of cluster asphericity at large radii may also become important.

Hence a successful semi-analytic model of the spherical cluster pressure, if that is indeed a viable goal, at the least needs careful calibration using numerical simulations which accurately treat all of the effects. The variance of the average profiles also encodes important information that is manifested in the power spectrum. Our studies also show that simplified analytic models that employ hydrostatic gas models with a constant Γ necessarily overpredict the SZ power on large scales by up to a factor of two and predict an inconsistent shape of the SZ power spectrum. The alternative that we explore in a subsequent paper is to use stacked scaled simulational clusters which are rotated to principal axes to provide the pressure form factors for the semi-analytic approach.

The tSZ power spectrum of our 512^3 simulation agrees well with the average of our ten 256^3 simulations. A large number of simulations are needed to properly sample the high-mass end of the cluster mass function and hence accurately deal with sample (cosmic) variance. Alternatively, larger cosmological volumes can compensate since they contain enough statistics on the large scale modes that are responsible in part for forming the highest-mass clusters which are also the rarest events. This, however, is quite challenging as we require the same (high-)resolution to accurately follow the physics in the cluster cores which is needed to obtain profiles that match current X-ray data. Our 256^3 simulations do not quite sample large enough scales to provide a fully converged kSZ power spectrum at low ℓ since we miss the long-wavelength tail of the velocity power spectrum. We also have ignored the patchy re-ionization kSZ which could be a significant contributor, up to 50% of the total kSZ (e.g., Iliev et al. 2008, 2007).

We have found the $\ell < 2000$ multipole range to be relatively insensitive to cooling and feedback, at least for the range constrained by the X-ray data. We did find the higher multipole range ($\ell \sim 2000 - 10000$) probed by the high-resolution ACT and SPT CMB telescopes is sensitive to the feedback prescription; hence the high-ℓ SZ power spectrum can be used to constrain the theory of intracluster gas, in particular for the highly uncertain redshifts > 0.8. In addition to the SZ power spectrum probe, our simulations can be used to address the cosmological significance of cluster counts as derived from the SZ effect. Counts provide complementary constraints on parameters that help to break some degeneracies that are present in the power spectrum method. By employing inhomogeneous, localized and self-regulated feedback we are not only able to match recent X-ray reconstructions of cluster core regions, but also decrease the tension in σ_8 estimated from SZ power with σ_8 from other cosmological probes. However, only a detailed confrontation between simulations exploring the vast terrain of feedback options with the rapidly improving high resolution observations of cluster interiors can move the theory of cluster gas physics and its use for precision cosmology forward.

We thank Norm Murray, Volker Springel, Hy Trac, Jerry Ostriker, Gil Holder, Niayesh Afshordi and Diasuke Nagai for useful discussions. Research in Canada is supported by NSERC and CIFAR. Simulations were run on SCINET and CITA's Sunnyvale HPC clusters.

REFERENCES

Afshordi, N., Lin, Y., Nagai, D., & Sanderson, A. J. R. 2007, MNRAS, 378, 293
Arnaud, M., Pratt, G. W., Piffaretti, R., Boehringer, H., Croston, J. H., & Pointecouteau, E. 2009, arXiv:0910.1234
Bhattacharya, S., Di Matteo, T., & Kosowsky, A. 2008, MNRAS, 389, 34
Bialek, J. J., Evrard, A. E., & Mohr, J. J. 2001, ApJ, 555, 597
Birkinshaw, M. 1999, Phys. Rep., 310, 97
Bode, P., Ostriker, J. P., & Vikhlinin, A. 2009, ApJ, 700, 989
Bond, J. R. et al. 2005, ApJ, 626, 12
Bond, J. R., Ruetalo, M. I., Wadsley, J. W., & Gladders, M. D. 2002, in Astronomical Society of the Pacific Conference Series, Vol. 257, AMiBA 2001: High-Z Clusters, Missing Baryons, and CMB Polarization, ed. L.-W. Chen, C.-P. Ma, K.-W. Ng, & U.-L. Pen, 15
Bondi, H., & Hoyle, F. 1944, MNRAS, 104, 273
Booth, C. M., & Schaye, J. 2009, MNRAS, 398, 53
Carlstrom, J. E., Holder, G. P., & Reese, E. D. 2002, ARA&A, 40, 643
Chatterjee, S., Di Matteo, T., Kosowsky, A., & Pelupessy, I. 2008, MNRAS, 390, 535
da Silva, A. C., Barbosa, D., Liddle, A. R., & Thomas, P. A. 2000, MNRAS, 317, 37
Duffy, A. R., Schaye, J., Kay, S. T., & Dalla Vecchia, C. 2008, MNRAS, 390, L64
Enßlin, T. A., Pfrommer, C., Springel, V., & Jubelgas, M. 2007, A&A, 473, 41
Fixsen, D. J., Cheng, E. S., Gales, J. M., Mather, J. C., Shafer, R. A., & Wright, E. L. 1996, ApJ, 473, 576
Fowler, J. W. et al. 2010, arXiv:1001.2934
Goldstein, J. H. et al. 2003, ApJ, 599, 773
Gonzalez, A. H., Zaritsky, D., & Zabludoff, A. I. 2007, ApJ, 666, 147
Holder, G. P., McCarthy, I. G., & Babul, A. 2007, MNRAS, 382, 1697
Iliev, I. T., Mellema, G., Pen, U., Bond, J. R., & Shapiro, P. R. 2008, MNRAS, 384, 863
Iliev, I. T., Pen, U., Bond, J. R., Mellema, G., & Shapiro, P. R. 2007, ApJ, 660, 933
Katz, N., & White, S. D. M. 1993, ApJ, 412, 455
Komatsu, E., & Seljak, U. 2002, MNRAS, 336, 1256
Komatsu, E. et al. 2010, arXiv:1001.4538
Kravtsov, A. V., Vikhlinin, A., & Nagai, D. 2006, ApJ, 650, 128
Larson, D. et al. 2010, arXiv:1001.4635
Lewis, A., & Bridle, S. 2002, Phys. Rev. D, 66, 103511
Lewis, G. F., Babul, A., Katz, N., Quinn, T., Hernquist, L., & Weinberg, D. H. 2000, ApJ, 536, 623
Lueker, M. et al. 2009, arXiv:0912.4317
Nagai, D., Kravtsov, A. V., & Vikhlinin, A. 2007, ApJ, 668, 1
Ostriker, J. P., Bode, P., & Babul, A. 2005, ApJ, 634, 964
Pfrommer, C., Enßlin, T. A., Springel, V., Jubelgas, M., & Dolag, K. 2007, MNRAS, 378, 385
Puchwein, E., Sijacki, D., & Springel, V. 2008, ApJ, 687, L53
Reichardt, C. L. et al. 2009, ApJ, 694, 1200
Roychowdhury, S., Ruszkowski, M., & Nath, B. B. 2005, ApJ, 634, 90
Scannapieco, E., Thacker, R. J., & Couchman, H. M. P. 2008, ApJ, 678, 674
Schäfer, B. M., Pfrommer, C., Bartelmann, M., Springel, V., & Hernquist, L. 2006, MNRAS, 370, 1309
Sehgal, N., Bode, P., Das, S., Hernandez-Monteagudo, C., Huffenberger, K., Lin, Y., Ostriker, J. P., & Trac, H. 2010, ApJ, 709, 920
Seljak, U., Burwell, J., & Pen, U. 2001, Phys. Rev. D, 63, 063001
Sievers, J. L. et al. 2009, arXiv:0901.4540

Sijacki, D., Pfrommer, C., Springel, V., & Enßlin, T. A. 2008, MNRAS, 387, 1403
Sijacki, D., & Springel, V. 2006, MNRAS, 366, 397
Sijacki, D., Springel, V., Di Matteo, T., & Hernquist, L. 2007, MNRAS, 380, 877
Spergel, D. N. et al. 2007, ApJS, 170, 377
Springel, V. 2005, MNRAS, 364, 1105
Springel, V., & Hernquist, L. 2003a, MNRAS, 339, 289
—. 2003b, MNRAS, 339, 312
Springel, V., White, M., & Hernquist, L. 2001, ApJ, 549, 681
Sunyaev, R. A., & Zeldovich, Y. B. 1970, Ap&SS, 7, 3
Thacker, R. J., Scannapieco, E., & Couchman, H. M. P. 2006, ApJ, 653, 86
Thompson, T. A., Quataert, E., & Murray, N. 2005, ApJ, 630, 167
Voit, G. M. 2005, Reviews of Modern Physics, 77, 207
White, M., Hernquist, L., & Springel, V. 2002, ApJ, 579, 16